Ab initio calculation of structural and lattice-dynamical properties of silicon carbide

K. Karch,* P. Pavone, W. Windl, O. Schütt, and D. Strauch
Theoretische Physik, Universität Regensburg, D-93040 Regensburg, Germany
(Received 11 April 1994; revised manuscript received 8 August 1994)

The plane-wave pseudopotential approach to density-functional theory (DFT) in the local-density approximation has been applied to investigate a variety of ground-state properties of the $3C$, $2H$, and $4H$ polytypes of silicon carbide. The linear-response theory within DFT has been used to obtain lattice-dynamical properties of cubic SiC such as the phonon-dispersion curves, phonon eigenvectors, elastic and Grüneisen constants, as well as the thermal expansion coefficient and specific heat within the quasiharmonic approximation. Finally, we present some results for phonon-dispersion curves in the hexagonal $2H$ (wurtzite) and $4H$ structure. These results are analyzed and discussed in view of further applications to temperature-dependent properties.

I. INTRODUCTION

Silicon carbide (SiC) is considered to be a promising material for electronic and optical devices due to its outstanding mechanical, chemical, thermal, and electronic properties. Microelectronic devices made of SiC can be used in high-power, high-speed, high-temperature, high-frequency, and even hard-radiation applications.[1,2] Yet, before a wide use of SiC in the production of electronic devices can be possible, a series of technological problems has to be solved, such as the growing of monocrystalline large-size and high-quality SiC samples or the doping with donors and acceptors. The overcoming of these technological problems requires a deep understanding of the physical properties peculiar to SiC. Furthermore, SiC is the only IV-IV compound which occurs not only in cubic ($3C$) but also in complex, long-range ordered hexagonal (nH) and rhombohedral (mR) structures. However, to date SiC has not been the subject of the same thorough theoretical and experimental investigations as, e.g., the group-IV crystals or the III-V semiconductors.

In recent years, first-principles investigations of the structural and electronic properties of SiC have been performed by many groups.[3–8] Further studies went deep into the high-pressure behavior[6,9] and the effects of atomic relaxation on structural properties[10,11] of SiC. Some attempts to explain the phenomenon of the polytypism of SiC have also been undertaken.[12–14] However, up to now only a few *ab initio* calculations of the lattice-dynamical properties of SiC are available.[5,15] Moreover, the thermal properties of SiC have not yet been investigated from first principles.

Since the electronic energies of the different phases of SiC are very close, inclusion of the phonon contributions to the free energy may become important and in this case these contributions must be calculated reliably. Thus the purpose of this work is a study of lattice-dynamical and thermal properties of some of the different phases of SiC, which need the structural properties as a prerequisite. Therefore, we have investigated various ground-state properties of the $3C$, $2H$, and $4H$ polytypes of SiC. We have calculated the equilibrium lattice parameters, the bulk modulus, the pressure derivative of the bulk modulus, the Born effective charges, and the high-frequency dielectric tensor. For cubic SiC, we have also calculated phonon-dispersion curves, phonon eigenvectors, elastic constants, and the internal-strain parameter. Concerning the hexagonal $2H$ and $4H$ phases, we have determined the phonon-dispersion curves along selected high-symmetry directions and the Γ point frequencies, respectively. Finally, we have evaluated the mode Grüneisen parameters, the thermal expansion coefficient, and the specific heat at constant volume and at constant pressure of $3C$ SiC within the framework of the quasiharmonic approximation. The results for all calculated quantities are in excellent agreement with the available experimental data.

The structure of the paper is the following: After this introduction a short outline of the theory and a brief description of the investigated physical quantities are given in Sec. II. In Sec. III the results of our calculation are presented and compared with the available experimental data. Finally, the conclusions are summarized in Sec. IV.

II. THEORETICAL FRAMEWORK

A. Method

The plane-wave pseudopotential total-energy scheme within the local-density approximation (LDA) of the density-functional theory is used to obtain the energy differences between the various structural phases of SiC. For the exchange and correlation energy the Perdew and Zunger[16] parametrization is used. The evaluation of integrals over the irreducible wedge of the Brillouin zone (BZ) has been performed using sets of Chadi-Cohen special points.[17] Soft norm-conserving pseudopotentials for carbon and silicon have been generated using the method proposed by Troullier and Martins.[18] Different potentials

have been constructed for different values of the angular momentum of the electrons ($l = 0, 1, 2$) in order to reproduce correct tails of the atomic wave functions, energy levels, and excitation energies for a number of electronic configurations of the single atoms. The obtained pseudopotentials yield phonon-dispersion curves for silicon and carbon elemental crystals[19] which are almost indistinguishable from those of Refs. 20 and 21, respectively.

Total-energy corrections to the second order in the lattice distortion corresponding to a given phonon are derived within the framework of the density-functional perturbation theory (DFPT) using the linear-response theory.[20–22] The DFPT is an efficient tool for the determination at any wave vector $\mathbf{q}$ in the BZ of the phonon frequencies and eigenvectors. The knowledge of these quantities is necessary for the calculation of physical quantities such as, e.g., the thermal expansion coefficient,[21] Raman-scattering cross section,[23,24] or infrared absorption spectra.[25] Using DFPT, the phonon frequencies and eigenvectors can be determined at *any* wave vector with a computational effort comparable to a ground-state calculation. This is an advantage compared with the frozen-phonon method, which restricts the calculations to high-symmetry points in the BZ.[26–28] A complete and detailed description of the numerical implementation of the DFPT formalism is given in Refs. 20 and 21.

B. Harmonic phonons

The displacement of an atom of the κth sublattice in the lth unit cell with the Bravais lattice vector $\mathbf{R}(l)$ can be written in the the form

$$u_\alpha \binom{l}{\kappa} = \frac{1}{\sqrt{m_\kappa}} u_\alpha(\kappa|\mathbf{q})\, e^{i[\mathbf{q}\cdot\mathbf{R}(l)-\omega(\mathbf{q})\,t]}, \tag{1}$$

where m_κ denotes the mass of the κth atom. Within the harmonic approximation the phonon frequencies $\omega_j(\mathbf{q})$ and eigenvectors $\boldsymbol{u}(\kappa|\mathbf{q}j)$ satisfy the secular equation

$$\sum_{\kappa'} \boldsymbol{D}\,(\kappa\kappa'|\mathbf{q})\;\boldsymbol{u}(\kappa'|\mathbf{q}j) = \omega_j^2(\mathbf{q})\,\boldsymbol{u}(\kappa|\mathbf{q}j)\,. \tag{2}$$

The expression for the dynamical matrix reads

$$D_{\alpha\beta}\,(\kappa\kappa'|\mathbf{q}) = \frac{1}{\sqrt{m_\kappa m_{\kappa'}}} \sum_l \frac{\partial^2 \mathcal{E}}{\partial u_\alpha\binom{0}{\kappa}\,\partial u_\beta\binom{l}{\kappa'}}\, e^{i\,\mathbf{q}\cdot\mathbf{R}(l)}\,, \tag{3}$$

where the second derivative of the total energy $\mathcal{E}$ of the crystal is evaluated at the equilibrium positions.

The total energy can be expressed as a sum of the direct ion-ion interaction energy $\mathcal{E}^{\rm ion}$ and the total ground-state electronic energy $\mathcal{E}^{\rm el}$ in the presence of the bare ionic potential $V(\mathbf{r}) = \sum_{l\kappa} V_\kappa\left[\mathbf{r} - \mathbf{R}\binom{l}{\kappa}\right]$. Therefore the dynamical matrix $D_{\alpha\beta}\,(\kappa\kappa'|\mathbf{q})$ can be separated into an ionic $D^{\rm ion}_{\alpha\beta}\,(\kappa\kappa'|\mathbf{q})$ and an electronic part $D^{\rm el}_{\alpha\beta}\,(\kappa\kappa'|\mathbf{q})$, where the ionic contribution can be evaluated in a straightforward way using Ewald's method.[29] The electronic part of the dynamical matrix is obtained from the Hellmann-Feynman theorem[30]

$$\sqrt{m_\kappa}\,D_{\alpha\beta}(\kappa\kappa'|\mathbf{q})\,\sqrt{m_{\kappa'}} = \frac{1}{N}\int \left(\frac{\partial\rho(\mathbf{r})}{\partial u_\alpha(\kappa|\mathbf{q})}\right)^* \frac{\partial V(\mathbf{r})}{\partial u_\beta(\kappa'|\mathbf{q})}\,d^3r + \delta_{\kappa\kappa'}\frac{1}{N}\int \rho(\mathbf{r})\frac{\partial^2 V(\mathbf{r})}{\partial u_\alpha(\kappa|\mathbf{q}=0)\partial u_\beta(\kappa|\mathbf{q}=0)}\,d^3r, \tag{4}$$

where N is the number of the unit cells in the lattice and $\partial\rho(\vec{r})\,/\partial u_\alpha(\kappa|\mathbf{q})$ is the linear response of the electronic system to a lattice distortion caused by a displacement of the κth sublattice. The linear response of the electronic system to a lattice distortion is calculated using first-order DFPT.

In polar compounds, the *long-range* part of the Coulomb interaction causes the splitting of the $\mathbf{q} = 0$ optic modes by raising the frequency of the LO mode above that of the TO modes. The *long-range* part of the Coulomb interactions corresponds to the macroscopic field arising from the ionic displacements. In the long-wavelength limit $\mathbf{q} \to 0$ the dynamical matrix is composed of the analytic (regular) and the nonanalytic (singular) part. The *analytic* part $\boldsymbol{D}^{\rm an}$ of the dynamical matrix for polar compounds is calculated in the same way as for the nonpolar compounds, neglecting any macroscopic polarization. The *nonanalytic* part of the dynamical matrix can be written as[31]

$$D^{\rm na}_{\alpha\beta}\,(\kappa\kappa'|\mathbf{q}\to 0) = \frac{4\pi}{\Omega\sqrt{m_\kappa m_{\kappa'}}}\frac{(\mathbf{Z}^B_\kappa\cdot\hat{\mathbf{q}})_\alpha\,(\hat{\mathbf{q}}\cdot\mathbf{Z}^B_{\kappa'})_\beta}{\hat{\mathbf{q}}\cdot\boldsymbol{\epsilon}_\infty\cdot\hat{\mathbf{q}}}\,, \tag{5}$$

where Ω denotes the volume of the unit cell, $\boldsymbol{\epsilon}_\infty$ the high-frequency dielectric tensor, and $\mathbf{Z}^B_\kappa$ the Born effective charge tensor for the κth ion in the unit cell. Both quantities are calculated self-consistently in the framework of first-order DFPT.[22,20]

A complete description of lattice dynamics requires the knowledge of the phonon eigenvectors of the dynamical matrix in addition to that of the eigenfrequencies. For SiC in the zinc blende structure, the vibrational modes with wave vectors along high-symmetry directions [100] (Δ) and [111] (Λ) can be classified as purely transverse or longitudinal, so that for acoustic modes one can write

$$\begin{aligned}\boldsymbol{u}^{(\rm C)}(\mathbf{q}\,j) &= c_j(\mathbf{q})\;\exp\left[i\phi_j(\mathbf{q})\right]\,\boldsymbol{e}_j\,,\\ \boldsymbol{u}^{(\rm Si)}(\mathbf{q}\,j) &= \sqrt{1-c_j^2(\mathbf{q})}\;\;\boldsymbol{e}_j\,,\end{aligned} \tag{6}$$

where $c_j(\mathbf{q})$ is the modulus of the eigenvectors, $\boldsymbol{e}_j$ is a real longitudinal or transverse unit vector, and $\phi_j(\mathbf{q})$ is a real phase function [with $\phi_j(\mathbf{q}) = 0$ for $\mathbf{q} = 0$]. The eigenvectors of the optical modes are obtained from Eq. (6) with an exchange of the amplitudes of the two atoms and simultaneous increase of the phase function by π.

C. Elastic properties of 3C SiC

The linear elastic constants $\boldsymbol{c}$ are defined as

$$c_{\alpha\beta,\gamma\delta} = \frac{\partial \sigma_{\alpha\beta}}{\partial \eta_{\gamma\delta}}, \tag{7}$$

where $\boldsymbol{\sigma}$ denotes the externally applied stress and $\boldsymbol{\eta}$ the strain. In the case of cubic crystals symmetry relations reduce the number of independent elastic constants to three: $c_{11} = c_{xx,xx}$, $c_{12} = c_{xx,yy}$, and $c_{44} = c_{yz,yz}$. The elastic constants c_{11} and c_{12} for a cubic crystal can be obtained by considering a crystal uniaxially strained along the [100] direction, and calculating the induced stress in [100] for c_{11} and in [010] direction for c_{12}.

For the zinc blende structure the evaluation of the shear constant c_{44} is more complicated: A uniform strain along the [111] direction causes the bond along [111] to be inequivalent to the other ones along $[\bar{1}\bar{1}1]$, $[\bar{1}1\bar{1}]$, and $[1\bar{1}\bar{1}]$. Under the action of this strain the distance of the nearest neighbors along the [111] direction is compressed by an amount of $(1-\zeta)\,\eta\, a_0\sqrt{3}/4$, where ζ is the internal-strain parameter.[32] The elastic constant c_{44} is given by[33]

$$c_{44} = c_{44}^0 - \frac{1}{4a_0}\,\mu\,\omega_{\mathrm{TO}}^2(\Gamma)\,\zeta^2, \tag{8}$$

where c_{44}^0 is the elastic constant in the absence of any internal displacements (i.e., $\zeta = 0$), μ is the reduced mass of the two atoms in the unit cell, and ω_{TO} the transverse zone-center phonon frequency. The internal-strain parameter ζ is the only independent component of the internal-strain tensor $\boldsymbol{\Delta}$ of the zinc blende structure,

$$\Delta_{\alpha\beta\delta}(1) = -\Delta_{\alpha\beta\delta}(2) = -\zeta\frac{a_0}{4}|\epsilon_{\alpha\beta\delta}|, \tag{9}$$

where $\epsilon_{\alpha\beta\delta}$ is the fully antisymmetric Levi-Civita tensor. ζ can be evaluated with three different procedures:[21] (i) using the dependence of the phase function $\phi_L(\mathbf{q})$ upon the wave vector $\mathbf{q} = 2\pi/a_0\,(\xi,\xi,\xi)$ for the longitudinal acoustic mode along the [111] direction,[34]

$$\zeta = \frac{3}{2} - \frac{1}{\pi}\left(\frac{\partial\phi_L(\xi)}{\partial\xi}\right)_{\xi=0}, \tag{10}$$

(ii) calculating the strain derivative of the force $\boldsymbol{F}(\kappa)$ acting on the κth atom at the equilibrium position,

$$\Delta_{\alpha\beta\delta}(\kappa) = \frac{1}{\mu\,\omega_{\mathrm{TO}}^2(\Gamma)}\left(\frac{\partial F_\alpha(\kappa)}{\partial\eta_{\beta\delta}}\right)_{u=0}, \tag{11}$$

(iii) determining the derivative of the strain $\boldsymbol{\sigma}$ with respect to the atomic displacements $\boldsymbol{u}$ at vanishing strain $\boldsymbol{\eta}$,

$$\Delta_{\alpha\beta\delta}(\kappa) = \frac{a_0^3}{4N\,\mu\,\omega_{\mathrm{TO}}^2(\Gamma)}\left(\frac{\partial\sigma_{\beta\delta}}{\partial u_\alpha(\kappa)}\right)_{\eta=0}. \tag{12}$$

D. Thermal expansion

Within a purely harmonic theory many important physical properties of solids such as thermal expansion, temperature dependence of the elastic constants, and phonon frequencies or finite phonon lifetimes cannot be described. However, for many purposes temperature-dependent properties of an anharmonic crystal can be studied within the so-called quasiharmonic approximation (QHA). In the QHA the interatomic force constants are renormalized by taking into account an explicit dependence upon the volume.

The harmonic equilibrium lattice parameters of a crystal are obtained by minimizing the total ground-state energy $\mathcal{E}(V)$. The structural parameters at finite temperature are defined by the minimum of the Helmholtz free energy $F(T,V)$. Within the QHA the Helmholtz free energy is given by

$$F(T,V) \overset{\mathrm{QHA}}{\cong} \mathcal{E}(V) + \sum_{\mathbf{q},j}\frac{1}{2}\hbar\omega_j(\mathbf{q},V) + \sum_{\mathbf{q},j} k_B T \ln\left[1-\exp\left(-\frac{\hbar\omega_j(\mathbf{q},V)}{k_B T}\right)\right]. \tag{13}$$

The linear thermal expansion coefficient for a cubic crystal can be written within QHA as[35,21]

$$\alpha(T) = \frac{1}{3B_0}\sum_{\mathbf{q},j}\gamma_j(\mathbf{q})\,c_{Vj}(\mathbf{q},T), \tag{14}$$

where $\gamma_j(\mathbf{q})$ is the mode Grüneisen parameter,

$$\gamma_j(\mathbf{q}) = -\frac{V_0}{\omega_j(\mathbf{q},V_0)}\left(\frac{\partial\omega_j(\mathbf{q},V)}{\partial V}\right)_{V=V_0}, \tag{15}$$

and c_{Vj} is the mode contribution to the specific heat at constant volume,

$$c_{Vj}(\mathbf{q},T) = \frac{\hbar\omega_j(\mathbf{q},V_0)}{V_0}\frac{\partial}{\partial T}\left[\exp\left(\frac{\hbar\omega_j(\mathbf{q},V_0)}{k_B T}\right)-1\right]^{-1}. \tag{16}$$

The specific heat $C_V(T)$ of the harmonic crystal is given by

$$C_V(T) = \sum_{\mathbf{q},j} c_{Vj}(\mathbf{q},T). \tag{17}$$

At the Γ point ($\mathbf{q} = 0$) the acoustic phonon frequencies vanish, and the mode Grüneisen parameters of the acoustic modes are nonanalytic. In the long-wavelength limit the Taylor expansion of the acoustic phonon frequencies and their derivatives with respect to the volume leads at the Γ point to the Grüneisen parameters[36]

$$\gamma_{\hat{\mathbf{q}}}(\Gamma) = \frac{1}{3}\left(1 - \left.\frac{\partial \ln v_{\hat{\mathbf{q}}}(V)}{\partial \ln V}\right|_{V_0}\right), \tag{18}$$

where $v_{\hat{\mathbf{q}}}(V)$ is the sound velocity in the direction of $\mathbf{q}$.

III. RESULTS

A. Structural properties

All calculations have been performed using a kinetic-energy cutoff of 48 Ry and equivalent sets of special

points for the different structures. The zinc blende lattice has been treated as a hexagonal structure in order to minimize numerical errors. The total energy has been calculated using six special points for the $4H$, 12 points for the $3C$, and 18 points for the $2H$ SiC. The equilibrium lattice properties have been obtained by minimizing the crystal total energy $\mathcal{E}(V)$ as a function of the structural parameters. The calculated crystal total energies at different volumes were fitted to the Vinet equation of state.[37] It has been found that the hexagonal $4H$ structure has the lowest energy, followed by the zinc blende structure and the wurtzite structure. The crystal total energies per Si-C pair are nearly identical: $\mathcal{E}^{2H}_{\rm min} - \mathcal{E}^{3C}_{\rm min} = 3.6 \times 10^{-4}$ Ry and $\mathcal{E}^{2H}_{\rm min} - \mathcal{E}^{4H}_{\rm min} = 5.6 \times 10^{-4}$ Ry. Likewise, the calculated equilibrium volumes of the SiC phases differ by less than 0.2%.

Because of the predominantly covalent bonding character in all SiC polytypes each atom of one kind is tetrahedrally surrounded by four atoms of the other kind. The polytypism arises through variants in the arrangement of these regular tetrahedra.[38] As all polytypes have the same nearest-neighbor shell, the first difference occurs with the second neighbors. Because of the similarity of the structures of SiC polytypes the differences in the total energies, equilibrium volumes per Si-C pair, and charge densities along some selected planes are almost negligible. This also becomes evident in Fig. 1, where the valence charge densities along the zigzag bonds of the $3C$ and $2H$ SiC phases—the structures with $h = 0$ and $h = 100$ percentage hexagonality[39]—are compared; the corresponding charge densities of other hexagonal polytypes are also nearly identical.[19]

Results pertaining to the static properties of the cubic $3C$ and the hexagonal $2H$ and $4H$ structures are given in Table I together with the corresponding experimental data. The theoretical results are in good agreement with the experimental values. The close relationship between the different SiC phases becomes also apparent in the similarity of the traces of the dielectric matrices ϵ_∞ and of the Born effective charge tensors $\mathbf{Z}^B$ of the hexagonal $2H$ and $4H$ structures with the corresponding values of the zinc blende structure: $\frac{1}{3}\,\mathrm{Tr}(\epsilon_\infty)_{2H} = 7.01$, $\frac{1}{3}\,\mathrm{Tr}(\epsilon_\infty)_{4H} = 7.03$, with $(\epsilon_\infty)_{3C} = 6.97$; $\frac{1}{3}\,\mathrm{Tr}(\mathbf{Z}^B)_{2H} = 2.68$, $\frac{1}{3}\,\mathrm{Tr}(\mathbf{Z}^B)_{4H} = 2.71$, with $(Z^B)_{3C} = 2.72$. The directional dependence of both the dielectric matrices and the Born effective charges in the hexagonal structures arises from the crystal anisotropy, but the effect is weak.

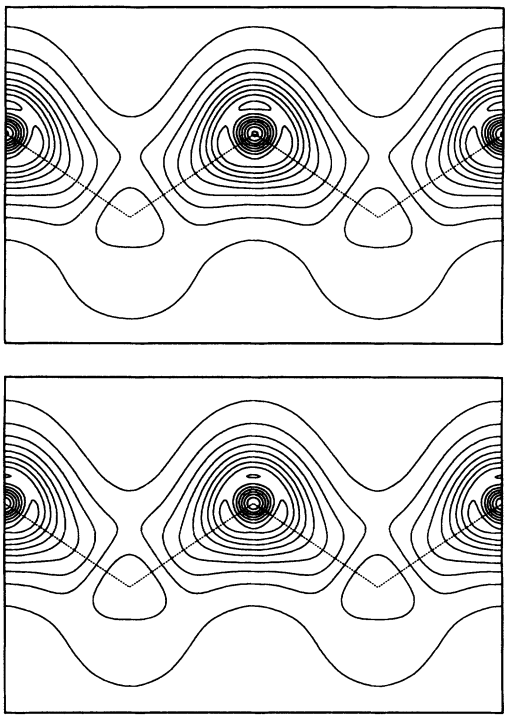

FIG. 1. Calculated valence charge density of the bond chains for the $3C$ (a) and $2H$ (b) phases of SiC. The contour interval is 0.2 $e/\text{Å}^3$. The maximum of the charge along the bonds is 1.96 ($3C$ SiC) and 1.92 ($2H$ SiC) $e/\text{Å}^3$. The dotted lines indicate the C-Si zigzag chain.

B. Phonon-dispersion curves

The theoretical phonon-dispersion curves of $3C$ SiC for several high-symmetry directions and the phonon density of states are shown in Fig. 2. Here a kinetic-energy cutoff of 44 Ry was used, and a set of ten special points in the irreducible BZ of the fcc lattice guaranteed converged values for the calculated frequencies within 1–2%. The dominant role of the carbon atom for the dynamics of $3C$ SiC is expressed by the behavior of the phonon-dispersion curves, which are more similar to those of diamond than to those of silicon. The flatness of the transverse acoustic modes near the BZ boundaries, which is typical for most of the tetrahedral semiconductors, does not appear in SiC, as in the case of diamond.[21] Another charac-

TABLE I. Equilibrium lattice constants a and c/a (a.u.), bulk modulus B_0 (Mbar), the derivative of the bulk modulus with respect to the pressure B_0', the tensor of the Born effective charge $\mathbf{Z}^B$, and the static dielectric tensor ϵ_∞ (in units of the elementary charge).

		a	c/a	B_0	B_0'	$(Z^B)_\parallel$	$(Z^B)_\perp$	$(\epsilon_\infty)_\parallel$	$(\epsilon_\infty)_\perp$
$3C$	Theory	8.21		2.22	3.88	2.72	2.72	6.97	6.97
	Expt.	8.24		2.24[a]		2.69[b]	2.69[b]	6.52[a]	6.52[a]
$2H$	Theory	5.80	1.64	2.24	3.75	2.62	2.81	6.89	7.27
	Expt.	5.81[a]	1.64[a]						
$4H$	Theory	5.81	3.27	2.23	3.66	2.64	2.84	6.96	7.17
	Expt.	5.80[a]	3.27[a]						

[a]Reference 50.
[b]Reference 51.

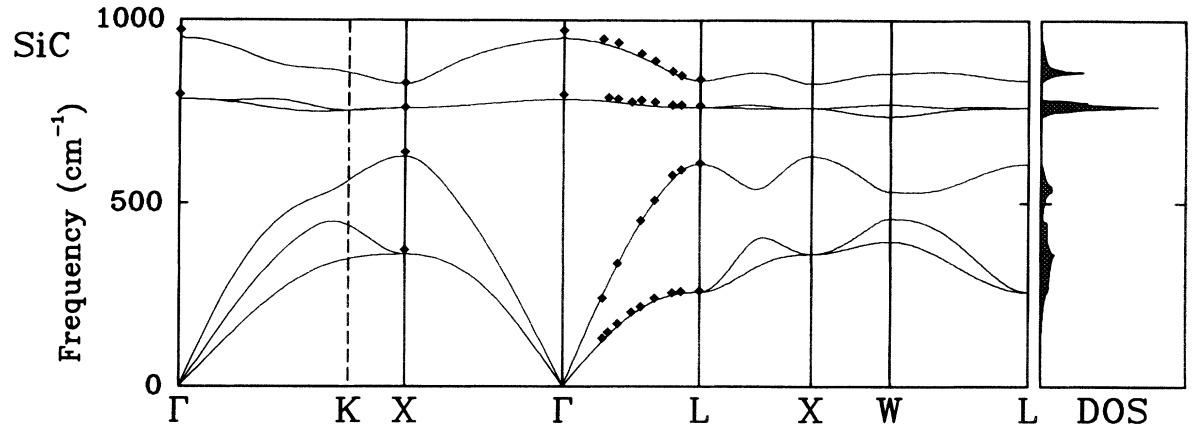

FIG. 2. Calculated phonon-dispersion curves and density of states (DOS) for 3C SiC. Experimental unfolded first-order Raman scattering data are denoted by diamonds (from Ref. 49).

teristic and peculiar feature of the dispersion curves of diamond—the overbending in the LO branch with a minimum at the Brillouin zone center[21,23]—does not appear in the dispersion curves of 3C SiC regardless of the strong influence of the carbon atom. In contrast to the diamond structure, the LO and TO modes are split at the Γ point because of the polar character of SiC, and, due to the mass difference, the LA and LO modes are split at the X point. The weak dispersion of the LO and TO phonon branches causes a gap and pronounced maxima in the optical range of the one-phonon density of states of 3C SiC. This peculiar behavior is rather uncommon to the tetrahedral III-V semiconductors. Numerical values for selected frequencies are given in Table II.

Experimental frequencies of SiC are available only from Raman-scattering results for various hexagonal and rhombohedral polytypes. After unfolding these data the calculated phonon frequencies agree excellently with the experimental ones. This agreement has been supported by recently measured second-order Raman spectra of 3C SiC, which have been theoretically reproduced using phonon frequencies and eigenvectors resulting from this work.[24]

For SiC in the wurtzite structure (2H SiC) the phonon frequencies of the ΓKM and the ΓA directions have been determined by interpolation of a set of dynamical matrices calculated along the respective directions. The calculated phonon-dispersion curves are compared with the available experimental data in Fig. 3. The directional dependence of the longitudinal optical modes at the Γ point is caused by the crystal anisotropy. However, the splitting is quite small, in agreement with the experimental value. Along the ΓA direction, which is the stacking direction, the phonon modes are folded. The sites of the silicon and the carbon atoms in the unit cell of 2H SiC are not equivalent under primitive lattice translations. However, time reversal, screw displacement, and glide reflection symmetries result in degeneracies of the phonon modes at the A point.[40]

The absence of energy gaps at the zone boundary suggests the use of the extended Jones zone, which contains only six phonon branches instead of 12. In Fig. 4 the calculated phonon-dispersion curves of SiC in the zinc blende structure along the [111] direction are plotted as solid lines and the unfolded curves of the wurtzite structure as dashed lines. The diamonds denote the unfolded Γ point frequencies of the 4H structure. The labels at the bottom of the figure correspond to the wurtzite structure and those at the top to the zinc blende structure. The wavelength of the phonon modes at the Γ$(2\pi/c)$ point in the wurtzite structure is $\lambda = 2\pi/q = c$; the two inequivalent silicon atoms in the unit cell and the inequivalent carbon atoms—each pair with a separation of $c/2$—vibrate with opposite phase. In contrast, in the Γ(0) mode these atoms vibrate in phase.

As discussed in Sec. III A, the different SiC polytypes have very similar valence charge densities along the stacking or the tetrahedral bonding direction; the same holds for ground-state energies and unit-cell volumes. The almost identical dynamical properties of the different SiC polytypes along the stacking direction as shown in Fig. 4 are related to their structural (static) similarity. These results confirm the experimentally deduced assumption that the dynamical properties of the different hexagonal SiC polytypes along the ΓA direction can be traced back to the dynamics of 3C SiC along the ΓL direction. This suggests that the short-range interactions are dominant for the static and dynamical properties and that minor

TABLE II. Phonon frequencies (in units of cm^{-1}) of 3C SiC at the high-symmetry points Γ, X, and L.

	Γ_{TO}	Γ_{LO}	X_{TA}	X_{LA}	X_{TO}	X_{LO}	L_{TA}	L_{LA}	L_{TO}	L_{LO}
Theory	783	956	366	629	755	829	261	610	766	838
Expt.[a]	795	972	372	639	760	829	261	610	765	837

[a]Reference 49.

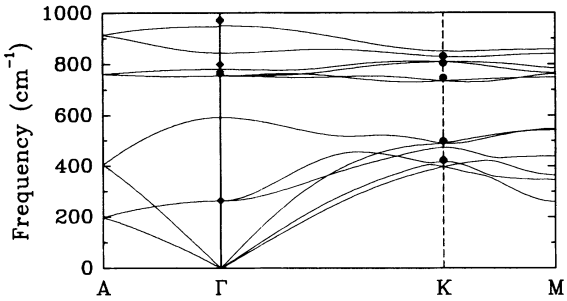

FIG. 3. Calculated phonon-dispersion curves for $2H$ SiC. Experimental Raman-scattering data at the Γ point are denoted by diamonds (from Ref. 53). The luminescence data (from Ref. 39) at the K point are denoted by full circles.

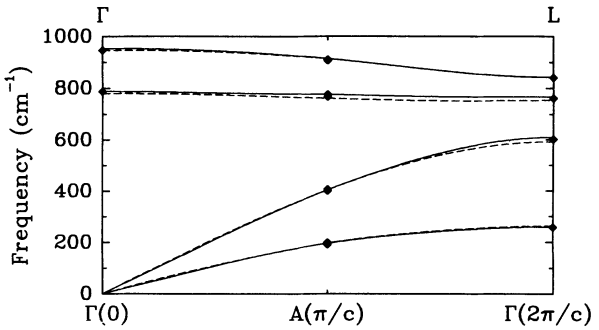

FIG. 4. Calculated phonon frequencies in the extended Jones zone for the stacking direction of the $3C$ (solid lines), $2H$ (dashed lines) and $4H$ (diamonds) SiC.

differences in the long-range Coulomb interactions are the reason for the appearance of polytypism.

C. Phonon eigenvectors in 3C SiC

The harmonic lattice dynamical properties of a crystal are incomplete without the phonon eigenvectors. The calculation of physical quantities such as infrared absorption, Raman spectra, or Debye-Waller factors involves the phonon frequencies as well as the eigenvectors. Even though the results for phonon frequencies derived with phenomenological models are often quite satisfactory, the associated eigenvectors differ usually significantly.[34,41] Thus predictions of eigenvectors from phenomenological models are unreliable. The *ab initio* results for the eigenvectors are not only important for the above-mentioned calculations but can also be used to judge the reliability of different phenomenological models.[36]

The calculated phase functions $\phi_j(\mathbf{q})$ of the eigenvectors, see Eq. (6), of $3C$ SiC for $\mathbf{q}$ along the high-symmetry directions Λ and Δ are shown in Fig. 5. The difference in the dynamics of SiC as compared to that of most of the other tetrahedral semiconductors is evident from the dependence of the phase function $\phi_L(\mathbf{q})$ of the longitudinal mode upon wave vector along the [111] direction. For comparison, the qualitatively different phase function of the longitudinal eigenvectors of silicon along the [111] direction, which is typical for the covalently bonded semiconductors, and that of diamond are included in Fig. 5. For symmetry reasons, the eigenvectors are real at the L point, so that only the two values 0 and π are allowed for ϕ_L. The case $\phi_L(L) = \pi$ corresponds to the so-called bond-stretching mode, in which the two atoms of a bond along the [111] direction vibrate with opposite phase. In contrast, the case $\phi_L(L) = 0$ corresponds to the bond-bending mode, in which the two atoms of this bond vibrate in phase.[36] In SiC and diamond the bond-bending mode has a higher frequency than the bond-stretching mode. The opposite holds for the typical semiconductors such as Si, Ge, or GaAs.[36] This peculiar behavior of the longitudinal phonon mode of $3C$ SiC and diamond along the [111] direction can be traced back to the strong bond-bending forces of these semiconductors.[21] The longitudinal phonon-dispersion curves of diamond, silicon, and $3C$ SiC along the Λ direction are shown in Fig. 6 together with the corresponding phases of the eigenvectors at the L point.

In the diamond structure the eigenvectors along the high-symmetry directions Λ and Δ are completely determined by the phase functions $\phi_j(\mathbf{q})$, because the amplitudes of the eigenvectors for the two atoms in the unit cell are equal, $c_j(\mathbf{q}) = 1/\sqrt{2}$. In the zinc blende structure, however, the knowledge of the amplitude $c_j(\mathbf{q})$ of the eigenvectors is necessary, too. The calculated amplitudes of the acoustic transverse and longitudinal eigenvectors of the carbon atom of $3C$ SiC along the [111] and [100] directions are shown in Fig. 7. The dispersion of the amplitude as a function of the wave vector $\mathbf{q}$ is caused by the different masses of the carbon and silicon atoms. The amplitude of the transverse modes shows quite a small dispersion in both directions Λ and Δ, whereas there is strong decrease of the amplitude of

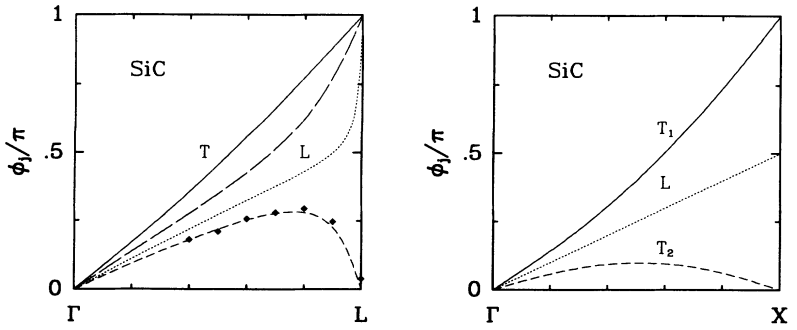

FIG. 5. Calculated eigenvector phase functions $\phi_j(\mathbf{q})$ of $3C$ SiC for $\mathbf{q}$ vector along the Λ and Δ direction for the transverse modes (solid lines) and longitudinal modes (dotted) lines. Along the [111] direction the longitudinal phase functions of diamond (long-dashed line) and silicon (short-dashed line) are included for comparison. The diamonds denote the experimental values of the longitudinal phase function of silicon from Ref. 34.

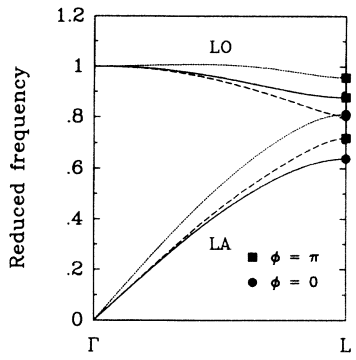

FIG. 6. Calculated longitudinal acoustic and optical phonon frequencies (in units of the Raman frequency) along the Λ direction for diamond (dotted lines), silicon (dashed lines), and the cubic phase of silicon carbide (solid lines). The respective phases of the eigenvectors at the L point are indicated.

the longitudinal eigenvectors with increasing $|\mathbf{q}|$. The amplitude of the longitudinal acoustic eigenvector of the carbon atom is nearly zero at the L point. Thus in the longitudinal acoustic mode at the L point almost the whole vibrational energy of the crystal is concentrated on the sublattice of the silicon atoms. For the longitudinal eigenvectors at the X point, symmetry requires that only one of the two different sublattices vibrates, even though it is *a priori* not clear which of the two atoms vibrates in which of the modes at the X point. It is generally assumed that the lighter atom vibrates with the higher frequency and vice versa. This is indeed brought out by the results shown in Fig. 7.

D. Internal-strain parameter of 3C SiC

For 3C SiC, the internal-strain parameter ζ has been determined using the three procedures which have been described in Sec. II C, see Eqs. (10)–(12). Once the phase $\phi_L(\mathbf{q})$ has been obtained, the first method is the simplest one numerically.

The second method involves the derivative of the stress tensor in the undistorted structure at zero macroscopic strain with respect to the displacement of one atom in the unit cell. In our case the atom at the origin of the unit cell has been kept fixed, while the other atom at the position $\tau_2 = a_0(1,1,1)/4$ has been displaced along the [111] direction. Such a displacement preserves the cubic symmetry of the lattice.

TABLE III. Theoretical values of the internal-strain parameter of 3C SiC derived (a) from the slope of the longitudinal phase function $\phi_L(\mathbf{q})$ at $\mathbf{q} = 0$, (b) from the strain derivative of the forces acting on the atoms, and (c) from the derivative of the stress with respect to the atomic displacements.

	(a)	(b)	(c)
ζ	0.379	0.378	0.383

Finally, the internal force $\boldsymbol{F}(\kappa)$ acting on the atoms converges slowly with respect to the kinetic-energy cutoff. Therefore the third method of calculation of the internal-strain parameter ζ from the strain derivative of the internal forces requires a higher kinetic-energy cutoff if the same accuracy is envisaged as in the other two methods. Another numerical disadvantage of this procedure is the lowering of the crystal symmetry due to the applied strain. Despite its disadvantages, this method has been used to get an independent value of the internal-strain parameter ζ. The internal forces acting on the atoms have been calculated by applying a uniform strain along the [111] direction. A kinetic-energy cutoff of 70 Ry has been used to achieve converged results for this method, whereas a kinetic-energy cutoff of 55 Ry is sufficient for the other two methods.

The calculated values of the internal-strain parameter of 3C SiC are given in Table III. To the best of our knowledge no experimental data for 3C SiC are available.

E. Elastic constants of 3C SiC

The calculation of the elastic constants from the stress calculations via Eq. (7) is easier than that from the total-energy calculations.[33,42] In this work the elastic constants of 3C SiC have been determined from self-consistent calculations in strained geometries using the stress theorem proposed by Nielsen and Martin.[33,43] The elastic constants c_{11} and c_{12} have been obtained directly from the slope of the independent components σ_{11} and $\sigma_{22} = \sigma_{33}$ of the stress tensor $\boldsymbol{\sigma}$ due to applied strain $\eta_{\alpha\beta} = \eta\delta_{\alpha 1}\delta_{\beta 1}$. The results for the stress components are shown for strain values of up to 2% in Fig. 8. There are no internal displacements of the atoms for stress along

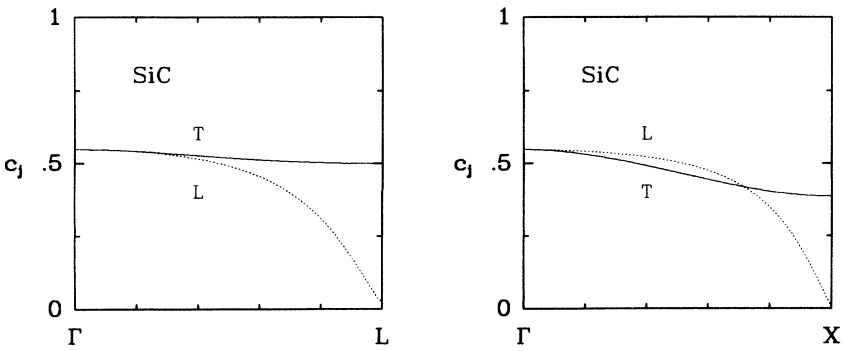

FIG. 7. Calculated amplitudes of the eigenvectors of the carbon atom in 3C SiC for vibrations with wave vector along the Λ and Δ direction for transverse (solid lines) and longitudinal modes (dotted lines).

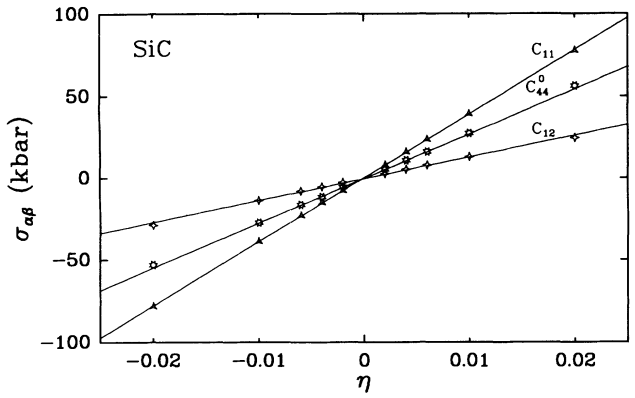

FIG. 8. Stress-strain relation in $3C$ SiC. η is the amplitude of the external strain. The symbols indicate calculated points, while the solid lines are linear least-squares fits. The theoretical values of the elastic constants c_{11}, c_{12}, and c_{44}^0 are given by the slopes of the plotted curves.

the [100] direction.

The calculation of the elastic constant c_{44} involves the internal strain as well, see Eq. (8). The clamped-ion term c_{44}^0 has been derived from the slope of the stress tensor caused by uniaxial strain along the [111] direction in absence of any internal displacements, see Fig. 8. The second term of Eq. (8) has been evaluated using an average value of the theoretical results for the internal-strain parameter ζ. The plots shown in Fig. 8 demonstrate that a linear relation between stress and strain is quite adequate for applied strain values of up to 2% in SiC. The calculated elastic constants of SiC are compared with the experimental data[44] in Table IV. The deviation between the theoretical and experimental values is less than 8%.

For an isotropic crystal the transverse sound velocity would be the same in all directions, and for cubic crystals one would get $c_{11} - c_{12} = 2c_{44}$. If the interatomic forces are central the number of independent elastic constants is reduced by the so-called *Cauchy relations*, in the case of cubic crystals $c_{12} = c_{44}$. The elastic constants of SiC neither meet the isotropy condition nor satisfy the Cauchy relation due to the presence of strong noncentral forces.

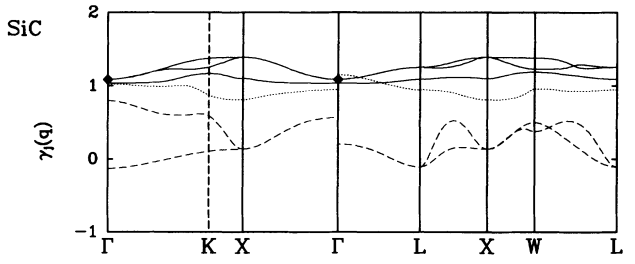

FIG. 9. Theoretical dispersion curves of the mode Grüneisen parameters $\gamma_j(\mathbf{q})$ of $3C$ SiC. Solid lines denote the optical modes, dotted lines the longitudinal acoustic modes, and dashed lines correspond to transverse acoustic modes (along the high-symmetry directions [100] and [111]). Diamonds denote the rescaled experimental data from Olego *et al.* (Ref. 51) using the theoretical values for B_0 and B_0'.

TABLE IV. Calculated values of the elastic constants and of the bulk modulus (in units of Mbar) of $3C$ SiC.

	c_{11}	c_{12}	c_{44}^0	c_{44}	B_0
Theory[a]	3.90	1.34	2.73	2.53	2.19[b]
Expt.[c]	3.90	1.42		2.56	2.24

[a]Derived from the stress-strain relation.
[b]Obtained from the relation $B_0 = (c_{11} + 2c_{12})/3$.
[c]The experimental data are derived by Lambrecht *et al.* (Ref. 52) from sound velocities of Feldman *et al.* (Ref. 49).

F. Mode Grüneisen parameters and thermal expansion coefficient of $3C$ SiC

In the QHA the anharmonic effects are taken into account by allowing the phonon frequencies to depend upon the volume. The volume dependence of the normal-mode frequencies has been derived by calculating the interatomic force constants and phonon frequencies for different unit-cell volumes around the equilibrium value.

The results for the mode Grüneisen parameters $\gamma_j(\mathbf{q})$, see Eq. (15), along several symmetry directions are plotted in Fig. 9. The mode Grüneisen parameters are predominantly positive with the exception of the small part of the lowest branches, corresponding to transverse acoustic modes, around the Γ and L points. This behavior of the Grüneisen parameters of $3C$ SiC is similar to that of diamond, for which all mode Grüneisen parameters are found to be positive,[21] and in contrast to that of silicon, for which almost the whole of the TA branches of the mode Grüneisen parameters are strongly negative.[19,36] Our result for the mode Grüneisen parameter of the TA branch at the X point [$\gamma_{\mathrm{TA}}(X) = 0.13$] is somehow higher than obtained from previous calculations [$\gamma_{\mathrm{TA}}(X) = -0.38$].[5] A similar discrepancy of theoretical results from different pseudopotentials has been observed in the case of Si.[19] The Bachelet-Hamann-Schlüter (BHS) pseudopotentials,[45] as used in Ref. 5, give TA Grüneisen constants for crystalline silicon which are more negative than those obtained from softer pseudopotentials;[46] according to Eq. (14), the Grüneisen constants from the BHS pseudopotentials lead to a thermal expansion coefficient of Si with a larger deviation from experiment in the low-temperature region, in contrast to those from softer pseudopotentials.

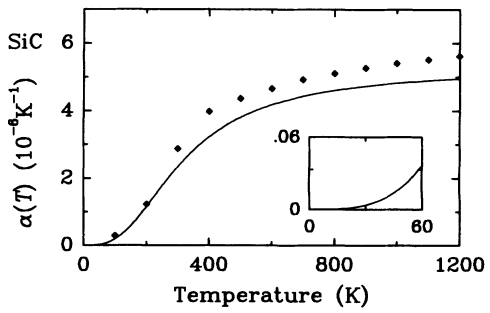

FIG. 10. Thermal expansion coefficient $\alpha(T)$ of $3C$ SiC as a function of temperature. Diamonds are experimental data from Ref. 54.

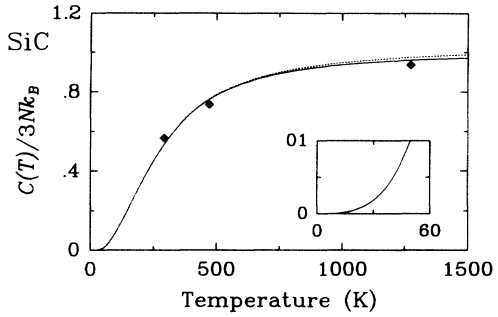

FIG. 11. Calculated specific heat at constant volume $C_V(T)$ (solid line) and at constant pressure $C_P(T) = C_V(T) + 9TV(T)B(T)\alpha^2(T)$ (dotted line) of $3C$ SiC as a function of temperature. Diamonds denote the experimental data for the specific heat $C_P(T)$ from Ref. 50. The difference between specific heat at constant pressure and at constant volume at a given temperature T has been determined using theoretically obtained values for $\alpha(T)$ and $B(T)$, see Ref. 48.

The thermal expansion coefficient of $3C$ SiC has been derived following Eq. (14) with results displayed in Fig. 10. The theoretical results are in good agreement with the experimental values keeping in mind the rather small relative volume change of the order of about 10^{-6} in the temperature range investigated. In the high-temperature regime all phonon modes are excited, and the thermal expansion coefficient tends to saturate at a constant value. The deviation between the theoretical and experimental data in the high-temperature range is probably caused by anharmonic effects of higher than third order which are not taken into account by the quasiharmonic approximation. As in the case of diamond and at variance with most of the other tetrahedral semiconductors, there is no temperature range with a negative thermal expansion coefficient. The negative expansion coefficient of silicon in the low-temperature regime is caused by the the negative contributions of the transverse acoustic modes of the mode Grüneisen parameters unlike in the case of SiC, where these contributions are too small.

The calculated specific heat at constant volume $C_V(T)$ and at constant pressure $C_P(T) = C_V(T) + 9TV\,B(T)\,\alpha^2(T)$ of $3C$ SiC is shown in Fig. 11. In the low-temperature region the difference between $C_V(T)$ and $C_P(T)$ is negligible, and it remains small also at higher temperatures due to the weak thermal expansion of this compound.

IV. CONCLUSIONS

We presented a first-principles calculation of static, dynamical, and thermal properties of three SiC polytypes within the pseudopotential approach to the density-functional theory in the local-density approximation. The ground-state properties of the cubic $3C$ and the hexagonal $2H$ and $4H$ polytypes of SiC have emerged to be very similar, especially concerning ground-state energies and volumes as well as the valence charge densities along the bonding and stacking directions.

Because of the very small energy differences between the investigated SiC phases reliable theoretical predictions about thermodynamic stability and possible temperature- and pressure-induced phase transitions are only feasible if the contributions of the lattice vibrations to the total energy are taken into account. For instance, the inclusion of the energy contribution of the zero-point motion raises the static value of the lattice parameter of $3C$ SiC by about 0.3%.[48] On the other hand, these small energy differences could play an important role with respect to the relative stability of the different polytypes.[47] Despite longstanding interest, the phenomenon of polytypism of SiC is still not properly understood, and basically this reflects a lack of understanding of polytype stability.

In this context the investigation of the dynamical and thermal properties of these phases is relevant. The similarity of the structural properties leads also to resembling dynamical properties for the different structures, like effective charges or phonon-dispersion curves along the stacking direction. The directional dependence of the dispersion curves at the Γ point, usually a fingerprint of uniaxiality, nearly vanishes. The phonon-dispersion curves of cubic SiC are intermediate between those of Si (with dispersion curves typical for most of the III-V compounds) and diamond, but definitely not their average. In addition to the rescaling of the frequencies by the different masses a rearrangement of the charge distribution takes place. Therefore, in contrast to the elemental crystals, SiC turns out to have a noticeable ionicity, i.e., charge asymmetry.[48]

Furthermore, several thermal properties of the $3C$ SiC have been derived using the quasiharmonic approximation, i.e., the specific heat at constant volume and at constant pressure as well as the thermal expansion coefficient and, as a by-product, the mode Grüneisen parameters. For these quantities first-principles results have been lacking so far, even though knowledge of them might be the key to a deeper understanding of the material properties of SiC and, consequently, of polytypism.

In fact, despite the generally excellent agreement of the theoretical results determined from the minimization of the total *static* energy with the available low-temperature experimental data, this procedure neglects the effects of the vibrational energy and entropy of the crystal. These effects should be included in a consistent *ab initio* calculation of the equilibrium properties at zero and finite temperature. From this point of view, this investigation of the lattice-dynamical properties is a fundamental preliminary step for a completely consistent description of the stability in these systems.

ACKNOWLEDGMENTS

The authors want to thank S. Baroni for the numerical support. This work has been supported by the Deutsche Forschungsgemeinschaft (Contract No. Schr123/8) and its Graduiertenkolleg (Contract No. Str118/10-1).

* Present address: Institut für Festkörpertheorie und Theoretische Optik, Friedrich-Schiller-Universität, D-07743 Jena, Germany.

[1] R. F. Davis, Z. Sitar, B. E. Williams, H. S. Kong, H. J. Kim, J. W. Palmour, J. A. Edmond, J. Ryu, J. T. Glass, and C. H. Carter, Jr., Mater. Sci. Eng. B **1**, 77 (1988).

[2] W. J. Choyke, in *The Physics and Chemistry of Carbides, Nitrides and Borides*, Vol. 185 of *NATO Advanced Study Institute, Series E: Applied Science*, edited by R. Freer (Kluwer, Dordrecht, 1990), p. 563.

[3] N. Churcher, K. Kunc, and V. Heine, Solid State Commun. **56**, 177 (1985).

[4] P. J. H. Dentener and W. van Haeringen, Phys. Rev. B **33**, 2831 (1986).

[5] N. Churcher, K. Kunc, and V. Heine, J. Phys. C **19**, 4413 (1986).

[6] B. H. Cheong, K. J. Chang, and M. L. Cohen, Phys. Rev. B **44**, 1053 (1991).

[7] V. I. Gavrilenko, S. I. Frolov, and N. I. Klyui, Physica B **185**, 349 (1993).

[8] C. H. Park, B.-H. Cheong, K.-H. Lee, and K. J. Chang, Phys. Rev. B **49**, 4485 (1994).

[9] K. J. Chang and M. L. Cohen, Phys. Rev. B **35**, 8196 (1987).

[10] C. Cheng, V. Heine, and R. J. Needs, J. Phys. Condens. Matter **2**, 1053 (1990).

[11] P. Käckell, B. Wenzien, and F. Bechsted (unpublished).

[12] C. Cheng, R. J. Needs, and V. Heine, J. Phys. C **21**, 1049 (1988).

[13] C. Cheng, V. Heine, and I. L. Jones, J. Phys. Condens. Matter **2**, 5097 (1990).

[14] C. Cheng, V. Heine, and R. J. Needs, Europhys. Lett. **12**, 69 (1990).

[15] C. Cheng, K. Kunc, and V. Heine, Phys. Rev. B **39**, 5892 (1989).

[16] J. P. Perdew and A. Zunger, Phys. Rev. B **23**, 5048 (1981).

[17] D. J. Chadi and M. L. Cohen, Phys. Rev. B **8**, 5747 (1973).

[18] N. Troullier and J. L. Martins, Phys. Rev. B **43**, 1993 (1991).

[19] K. Karch, Ph.D. thesis, Universität Regensburg, 1993.

[20] P. Giannozzi, S. de Gironcoli, P. Pavone, and S. Baroni, Phys. Rev. B **43**, 7231 (1991).

[21] P. Pavone, K. Karch, O. Schütt, W. Windl, D. Strauch, P. Giannozzi, and S. Baroni, Phys. Rev. B **48**, 3156 (1993).

[22] S. Baroni, P. Giannozzi, and A. Testa, Phys. Rev. Lett. **58**, 1861 (1987).

[23] W. Windl, P. Pavone, K. Karch, O. Schütt, D. Strauch, P. Giannozzi, and S. Baroni, Phys. Rev. B **48**, 3164 (1993).

[24] W. Windl, K. Karch, P. Pavone, O. Schütt, D. Strauch, W. H. Weber, K. C. Hass, and L. Rimai, Phys. Rev. B **49**, 8764 (1994).

[25] H. Sterner, W. Windl, K. Karch, P. Pavone, O. Schütt, and D. Strauch (unpublished).

[26] H. Wendel and R. M. Martin, Phys. Rev. B **19**, 5251 (1979).

[27] K. Kunc and R. M. Martin, Phys. Rev. Lett. **48**, 406 (1982).

[28] M. T. Yin and M. L. Cohen, Phys. Rev. B **26**, 3259 (1982).

[29] P. P. Ewald, Ann. Phys. (Leipzig) **64**, 253 (1921).

[30] H. Hellmann, *Einführung in die Quantenchemie* (Deuticke, Leipzig, 1937); R. P. Feynman, Phys. Rev. **56**, 340 (1939).

[31] W. Cochran and R. A. Cowley, J. Phys. Chem. Solids **23**, 447 (1962).

[32] L. Kleinman, Phys. Rev. **128**, 2614 (1962).

[33] O. H. Nielsen and R. M. Martin, Phys. Rev. Lett. **50**, 697 (1983).

[34] D. Strauch, A. P. Mayer, and B. Dorner, Z. Phys. B **78**, 405 (1990).

[35] T. H. K. Barron, J. G. Collins, and G. K. White, Adv. Phys. **29**, 609 (1980).

[36] P. Pavone, Ph.D. thesis, SISSA-ISAS, Trieste, 1991.

[37] P. Vinet, J. Ferrante, J. R. Smith, and J. H. Rose, J. Phys. C **19**, L467 (1986); P. Vinet, J. H. Rose, J. Ferrante, and J. R. Smith, J. Phys. Condens. Matter **1**, 1941 (1989).

[38] G. C. Trigunayat and G. K. Chadha, Phys. Status Solidi A **4**, 9 (1971).

[39] L. Patrick, D. R. Hamilton, and W. J. Choyke, Phys. Rev. **143**, 526 (1966).

[40] G. F. Koster, in *Solid State Physics: Advances in Research Applications*, edited by F. Seitz and D. Turnbull (Academic, New York, 1957), Vol. 5.

[41] R. S. Leigh, B. Szigeti, and V. K. Tewary, Proc. R. Soc. London Ser. A **320**, 505 (1971).

[42] M. Kitamura and W. A. Harrison, Phys. Rev. B **44**, 7941 (1991).

[43] For piezoelectric structures, like zinc-blende structure, it is necessary to specify the electric boundary conditions. In this work the elastic constants are calculated using vanishing macroscopic electric fields. The piezoelectric effects, which require the inclusion of the macroscopic fields, are not considered.

[44] The elastic constants have been determined from experimental sound velocities (see Ref. 49) of hexagonal SiC polytypes. Up to now, to the best of our knowledge there has been no direct measurement of the full set of elastic constants of 3*C* SiC.

[45] G. B. Bachelet, D. R. Hamann, and M. Schlüter, Phys. Rev. B **26**, 4199 (1982).

[46] P. Pavone and S. Baroni (unpublished).

[47] W. H. Backes, P. A. Bobbert, and W. van Haeringen, Phys. Rev. B **49**, 7564 (1994).

[48] K. Karch, P. Pavone, W. Windl, D. Strauch, and F. Bechstedt, *Proceedings of the 1994 Satellite Symposium on Thirty Years of Density-Functional Theory, Cracow, Poland, 1994* (Wiley, New York, 1994), p. 1.

[49] D. W. Feldman, J. H. Parker, Jr., W. J. Choyke, and L. Patrick, Phys. Rev. **173**, 787 (1968).

[50] *Physics of Group-IV and III-V Compounds*, edited by O. Madelung, Landolt-Börnstein, New Series, Group III, Vol. 17, Pt. a (Springer-Verlag, Berlin, 1982).

[51] D. Olego, M. Cardona, and P. Vogl, Phys. Rev. B **25**, 3878 (1982).

[52] W. R. L. Lambrecht, B. Segall, M. Methfessel, and M. van Schilfgaarde, Phys. Rev. B **44**, 3685 (1991).

[53] S. Nakashima, A. Wade, and Z. Inoue, J. Phys. Soc. Jpn. **56**, 3375 (1987).

[54] A. Taylor and R. M. Jones, in *Silicon Carbide — A High Temperature Semiconductor*, edited by J. R. O'Connor and J. Smiltens (Pergamon Press, Oxford, 1960).

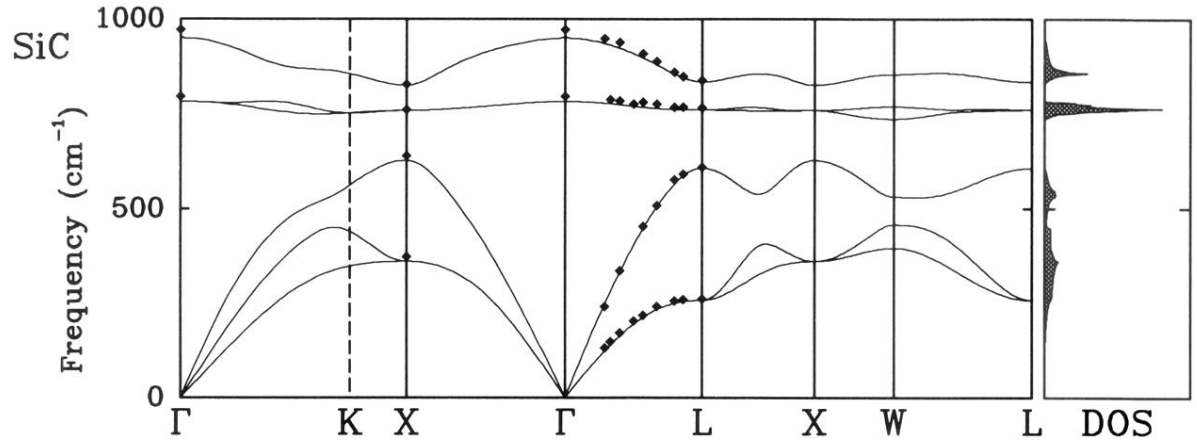

FIG. 2. Calculated phonon-dispersion curves and density of states (DOS) for 3*C* SiC. Experimental unfolded first-order Raman scattering data are denoted by diamonds (from Ref. 49).